Research article

Eduardo Martínez Castellano, Julen Tamayo-Arriola, Miguel Montes Bajo, Alicia Gonzalo, Lazar Stanojević, Jose María Ulloa, Oleksii Klymov, Javier Yeste, Said Agouram, Elías Muñoz, Vicente Muñoz-Sanjosé and Adrian Hierro*

Self-assembled metal-oxide nanoparticles on GaAs: infrared absorption enabled by localized surface plasmons

https://doi.org/10.1515/nanoph-2021-0167
Received April 14, 2021; accepted June 4, 2021;
published online June 18, 2021

Abstract: Metal-oxides hold promise as superior plasmonic materials in the mid-infrared compared to metals, although their integration over established material technologies still remains challenging. We demonstrate localized surface plasmons in self-assembled, hemispherical CdZnO metal-oxide nanoparticles on GaAs, as a route to enhance the absorption in mid-infrared photodetectors. In this system, two localized surface plasmon modes are identified at 5.3 and 2.7 μm, which yield an enhancement of the light intensity in the underlying GaAs. In the case of the long-wavelength mode the enhancement is as large as 100 near the interface, and persists at depths down to 50 nm. We show numerically that both modes can be coupled to infrared intersubband transitions in GaAs-based multiple quantum wells, yielding an absorbed power gain as high as 5.5, and allowing light absorption at normal incidence. Experimentally, we demonstrate this coupling in a nanoparticle/multiple quantum well structure, where under *p*-polarization the intersubband absorption is enhanced by a factor of 2.5 and is still observed under *s*-polarization, forbidden by the usual absorption selection rules. Thus, the integration of CdZnO on GaAs can help improve the figures of merit of quantum well infrared photodetectors, concept that can be extended to other midinfrared detector technologies.

Keywords: CdO; intersubband transition; localized surface plasmon; metal-oxide; quantum well.

***Corresponding author: Adrian Hierro**, ISOM, Universidad Politécnica de Madrid, Madrid, Spain, E-mail: adrian.hierro@upm.es. https://orcid.org/0000-0002-0414-4920

Eduardo Martínez Castellano, Julen Tamayo-Arriola, Miguel Montes Bajo, Alicia Gonzalo, Lazar Stanojević, Jose María Ulloa and Elías Muñoz, ISOM, Universidad Politécnica de Madrid, Madrid, Spain. https://orcid.org/0000-0003-0888-160X (E. Martínez Castellano). https://orcid.org/0000-0002-5701-0264 (J. Tamayo-Arriola). https://orcid.org/0000-0002-9352-5820 (M. Montes Bajo). https://orcid.org/0000-0002-8449-388X (A. Gonzalo). https://orcid.org/0000-0002-1478-514X (L. Stanojević). https://orcid.org/0000-0002-5679-372X (J.M. Ulloa)

Oleksii Klymov, Javier Yeste, Said Agouram and Vicente Muñoz-Sanjosé, Departament de Física Aplicada i Electromagnetisme, Universitat de València, Burjassot, Spain. https://orcid.org/0000-0003-2734-5028 (O. Klymov). https://orcid.org/0000-0002-2338-4575 (J. Yeste). https://orcid.org/0000-0002-9906-1174 (S. Agouram). https://orcid.org/0000-0002-3482-6957 (V. Muñoz-Sanjosé)

1 Introduction

In recent years, the field of plasmonics is undergoing an accelerated transformation due to the confluence of multiple technological advances. The latest developments in nanolithography have allowed the realization of nanostructured metasurfaces and plasmonic nanoparticles with an extreme level of precision, allowing to tackle a wide range of applications, including biosensing and fingerprinting, solar cells, photodetectors and modulators, perfect absorbers, or filters and phase shifters [1–4]. Together with these technological advances, the other great revolution in plasmonics comes from the development of new materials that promise to improve the widely-used noble metals in those areas where they exhibit their weaknesses [5, 6], such as the infrared (IR) range of the spectrum [7]. These new materials, among which we highlight metal-oxides, promise new innovative approaches to old problems in IR photonics, such as IR photodetection and its poor signal/noise ratio.

Although IR photonics is currently a well-established field with a wide range of commercial and experimental applications including medicine, astronomy, and surveillance [8], commercial IR photodetectors still face unavoidable issues arising specifically in the mid-IR range.

When operating at room temperature, the thermal energy of the carriers (kT, with k Boltzmann's constant and T the temperature) becomes comparable to the energy of the optical transition involved in the IR detection, resulting in an increased thermal noise [9]. Different strategies have been developed to overcome this issue. Since light absorption decays exponentially in the material as $e^{-\alpha \cdot d}$, where α is the absorption coefficient and d the distance traveled by the light in the material, optimizing the material thickness according to this absorption law is the first step to improve the signal/noise ratio [8]. A common approach to further increase this ratio is to enhance light absorption in the detector through the use of lenses and reflectors [8], although they involve major drawbacks in terms of manufacturing costs and miniaturization possibilities.

In the last few decades, the field of plasmonics has provided an innovative approach to this problem [9], based on the field-enhancement properties of metallic nanostructures [4]. Plasma oscillations in a metal-photodetector interface allow subwavelength light confinement that leads to an improved absorption efficiency [9, 10]. Several metallic plasmonic nanopatterns such as gratings [11], perforated layers, [12] and nanorods [13] have been proven successful in this area. Metallic nanoparticles have also demonstrated their capability to support plasmonic modes (localized surface plasmons or LSP), with demonstrated field concentration in the ultraviolet (UV) or the visible range of the spectrum [4, 14]. However, targeting the mid-IR with noble metals exposes the limitations they exhibit in this range [15, 16]: Achieving a plasmonic response in the mid-IR requires complex lithography processes, as those previously quoted, and dealing with intrinsic material limitations, as the unavoidable intraband losses [7].

In order to circumvent the limitations of noble metals in the mid-IR, metal-oxides have been identified as the perfect candidates as plasmonic materials [7]. Among all metal-oxides, *n*-CdO stands out as the best available material with unprecedented figures of merit, specifically for LSPs in the 3–5 μm atmospheric window [17]. Indeed, *n*-CdO has a very high plasma frequency, which can be tuned via doping or alloying [18–20], and low optical losses [18–20]. The extraordinary properties of CdO can be further improved by introducing 10% of Zn to form a ternary compound, $Cd_{0.9}Zn_{0.1}O$, which presents a plasma frequency over 4000 cm^{-1} with low losses around 500 cm^{-1} [21].

Thus, we show in this paper how CdZnO nanoparticles (NPs) deposited on GaAs-based photodetectors can be used for enhanced light absorption in the 3–5 μm atmospheric window. GaAs is selected as the substrate due to its well-established position in photonics technology in the mid-IR, with a wide range of applications including lasers [22], solar cells [23], and IR photodetectors [8]. In this work, we present a detailed analysis of the LSP resonances in CdZnO NP systems with the prospect of their integration on GaAs-based photodetectors, with a special focus in quantum well IR photodetectors (QWIPs). The results from this work can be nevertheless applicable to other material systems absorbing in the mid-IR.

2 Deposition and geometry of the nanoparticles

Four GaAs samples covered by different NP densities are presented. The $Cd_{0.9}Zn_{0.1}O$ NP coatings were grown through a self-assembled process on semi-insulating GaAs substrates by metal-organic chemical vapor deposition (MOCVD). The same flux parameters were used for all samples at a growth temperature of 304 °C. The NP size and the substrate coverage ratio were controlled by increasing the growth time from 90 to 420 s.

The scanning electron microscope (SEM) images of the four samples are shown in Figure 1. For the lower growth times, the covered area of the substrate and the average NP radius were calculated via image analysis, assuming the NP shape to be close to a perfect

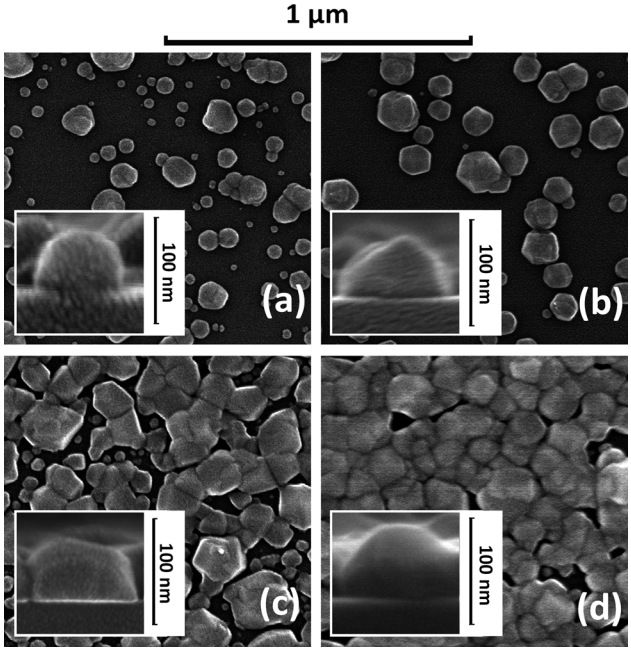

Figure 1: Plan-view SEM images of the $Cd_{0.9}Zn_{0.1}O$ NPs grown on semi-insulating GaAs substrates with increasing growth time and surface coverage.
(a) 90 s (growth time) – 25% (coverage), (b) 180 s – 32%, (c) 225 s – 68%, and (d) 420 s – 86%. The insets show the cross-sectional views of single NPs.

hemisphere. The surface coverage and NP size was 25% and 34 nm, for the 90 s sample, and 32% and 60 nm, for the 180 s sample. The samples with longer growth times (225 and 420 s) resulted in high surface coverage ratios (68 and 86%, respectively), but the NPs can no longer be considered as isolated due to the high degree of coalescence.

3 Characterization of the plasmonic response

The plasmonic response of the samples was measured in a Fourier transform infrared (FTIR) spectrometer in a *p*-polarized transmittance geometry. For each sample, the angle of incidence was controlled ranging from normal incidence up to 80°. The transmittance spectra of all samples were normalized by the transmittance of a bare semi-insulating GaAs substrate, hence isolating the effect due to the NP from that of the GaAs substrate. The transmittance curves for all samples are shown in Figure 2.

Starting with the samples with a substrate coverage of 25 and 32% (Figure 2(a) and (b)), two transmittance minima are easily identifiable. A low energy (LE) minimum is located around 1900 cm^{-1} (5.3 μm) and a high energy (HE) one around 3700 cm^{-1} (2.7 μm). Here, each mode presents a different angle-dependent behavior: The LE mode finds its minimum transmittance at normal incidence, while the HE mode is more pronounced at larger angles of incidence. Taking this into account, each minimum can be associated with a different direction of the plasma oscillation in the NP. In the LE mode, electric field oscillation occurs in the plane defined by the substrate interface, while the HE mode corresponds to an out-of-plane oscillation. Non-plasmonic absorption phenomena are not expected in the spectra, as the phonon resonances of GaAs and $Cd_{0.9}Zn_{0.1}O$ are located at energies well below the measured range [21, 24]. The appearance of these two different, well-defined modes, is a consequence of the broken symmetry of the system in contrast with the ideal spherical NP case [25]. When the surface coverage is increased beyond the coalescence of the NPs, the HE mode stays approximately unchanged, but the LE mode degrades (Figure 2(c) and (d)).

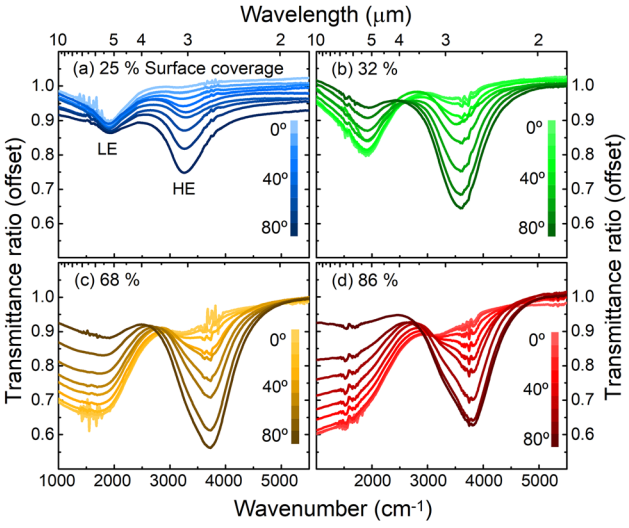

Figure 2: Measured transmittance curves at different angles of incidence (10° steps) for increasing NP substrate coverage. (a) 25%, (b) 32%, (c) 68%, and (d) 86%. The transmittance curves of the samples were normalized by the response of a bare semi-insulating GaAs substrate at the same angles of incidence.

To study the field distribution emerging from both plasmonic responses, the NP geometry was included in a Finite-difference time-domain (FDTD)-based model. For this purpose, we chose the sample with a substrate coverage of 32% since it is the sample with the sharpest and deepest resonances, and the SEM images still show that the NPs are mostly isolated. The simplified geometric model consists of an isolated, 60 nm-high, hemisphere-shaped NP on a GaAs substrate. Although the NP proximity could result in noticeable changes of the resonant frequencies due to near-field interactions (see Supplementary Material), very good results are obtained from our approach (Figure 3(a) and (b)) avoiding the increased modeling complexity derived from the real random distribution.

For the calculation, the semi-insulating GaAs substrate was modeled with a constant refractive index of 3.3 [26], and the dielectric function of $Cd_{0.9}Zn_{0.1}O$ was represented by the Drude model given by

$$\varepsilon_{\mathrm{CdZnO}}(\omega) = \varepsilon_{\infty}\left(1 - \omega_P^2/\left(\omega^2 + i\omega\gamma_P\right)\right) \quad (1)$$

where ε_{∞} is the high-frequency dielectric constant, ω_P is the plasma frequency, and γ_P is its associated optical damping. Values of $\varepsilon_{\infty} = 5.1$, $\omega_P = 4200$ cm^{-1} and $\gamma_P = 600$ cm^{-1} were chosen from those obtained by our group in $Cd_{0.9}Zn_{0.1}O$ thin films [20], which replicated with good accuracy the measured angle-dependent transmittance (Figure 3(a) and (b)).

The LE mode degradation observed at low energies (Figure 2(c) and (d)) can also be computationally approached. When NPs have coalesced as in Figure 1(d), the system can no longer be described by isolated NPs but as a thin, polycrystalline layer. Figure 3(c) represents this process of coalescence with NPs placed at the nodes of a 2D square periodic system. As the distance between NPs decreases, the system transmittance approaches that corresponding to a continuous thin film. For this final stage, the Drude model predicts intense reflection for

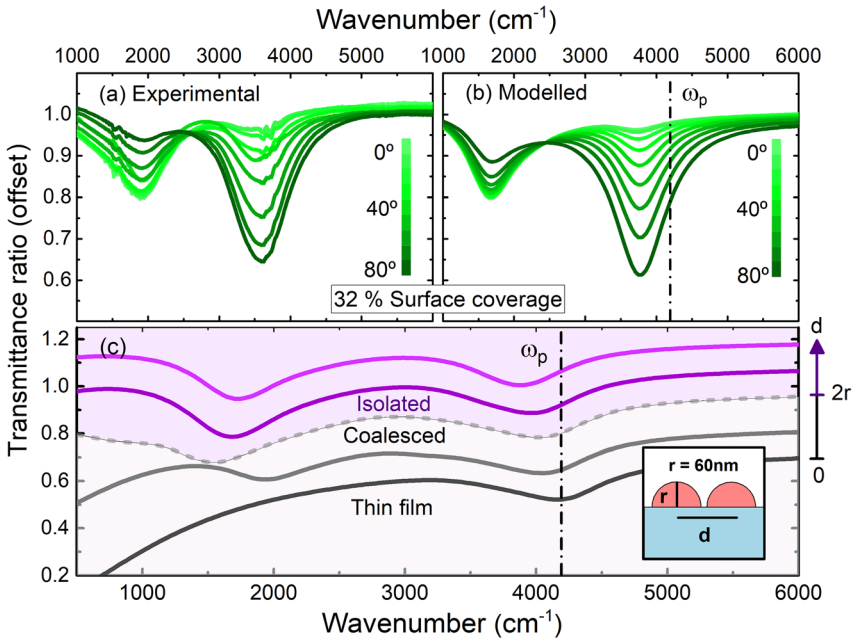

Figure 3: (a) Measured transmittance curves of the 32% surface coverage sample. (b) Computational transmittance curves from the isolated NP model with the same surface coverage. (c) 45° transmittance: Effect of near field interaction and coalescence in a periodic model. The curves in purple light field represent an uncoalesced stage with center-to-center distances (d in the figure) of 150 and 130 nm, larger than twice the radius of the NPs, $r = 60$ nm. Gray curves correspond to a coalesced stage with d values ranging from 120 (dashed line) to 0 nm (thin film limit) with an intermediate value of $d = 116$ nm.

frequencies below ω_P, which is the asymptotic limit of the HE mode frequency in a continuous thin film.

We next evaluate the distribution and enhancement of the electric field at resonant frequencies. To do so, we consider two systems consisting of a GaAs substrate with and without an isolated $Cd_{0.9}Zn_{0.1}O$ NP placed on its surface and surrounded by air. The electric field distribution is calculated for both systems for every point in 3D-space, and the enhancement factor of the square of the electric field (proportional to light intensity) is thus calculated as the ratio between these two cases. These results are shown in Figure 4 for three angles of incidence: Normal incidence for the LE mode, 80° for the HE mode (largest angle of incidence experimentally achievable), and 45° for both modes. The direction of the electric field is also represented in the latter two cases.

As observed in Figure 4(a) and (c), the LE mode exhibits strong magnification around the edges of the NP. This is fully compatible with in-plane oscillations of the plasma inside the NP as expected from the transmittance measurements, where this mode intensifies as the angle of incidence decreases. The electric field direction, represented in Figure 4(e), is highly consistent with these results. The charge accumulation at the vertices of the NPs in this mode results in a strong divergence of the field around them, with important out-of-plane electric field components in the GaAs substrate. By contrast, the enhancement of the electric field in the HE mode is observed mainly at the apex of the NP (Figure 4(b) and (d)), consistent with out-of-plane plasma oscillations, but there is also a small enhancement in the GaAs substrate. Figure 4(e) and (f) also illustrate that, for an angle of incidence of 45°, within the NP the LE and HE

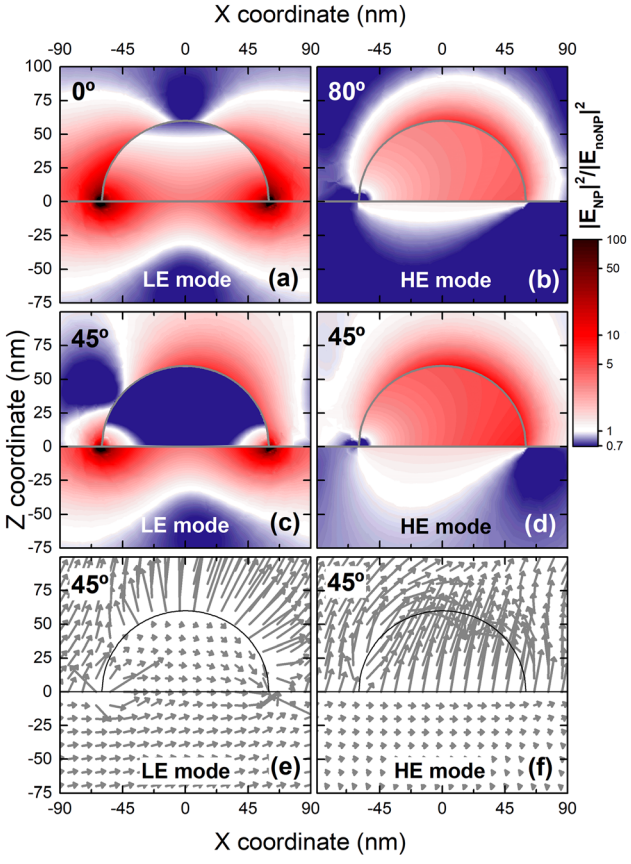

Figure 4: (a–d) Enhancement of the squared electric field, defined as the ratio of the squared module of the electric field with and without NPs, for both modes and different angles of incidence (0°, 45°, and 80°) in *p*-polarization. (e–f) Electric field vector at a 45° angle of incidence for the LE mode (e), and HE mode (f). Arrow lengths are proportional to the field module. The incident wave impinges from the top-left side of the images.

resonances are heavily polarized parallel and perpendicular to the NP/substrate interface, respectively.

From a practical perspective, the overall distribution and the penetration of the enhanced light intensity in the GaAs substrate is a key factor. The LE mode has a clear advantage over the HE one, with much higher enhancement and increased penetration depth and magnification values over a factor of 100 around the NP edge, decreasing to 1.2 at depths around 50 nm. Furthermore, this mode finds its best-case scenario at normal incidence, a desirable property for its integration on photodetectors. Conversely, the HE mode presents magnifications around 1.1 just below the surface, with no noticeable magnification at depths beyond 20 nm. If the out-of-plane component of the field is considered on its own, the HE mode reaches much better figures as will be discussed below.

4 Coupling of the NP plasmonic modes to quantum wells

The evaluation of the benefits of metal-oxide NPs on GaAs-based IR photodetection requires a complementary study of the increased power absorption by a functional absorbing system. To do so, we consider the use of $Cd_{0.9}Zn_{0.1}O$ NP coatings on GaAs/$Al_xGa_{1-x}As$ MQWs, which define the active region of QWIPs, a well-stablished technology in GaAs-based photodetection [8]. QWIPs rely on intersubband absorption in quantum wells, typically in the conduction band, and present absorption energies in the infrared [8], which can be made resonant with the LE and HE modes. Moreover, QWIPs may contain as few as five quantum wells [27] and thus can take full advantage of the field enhancement provided by the LSP modes. The relatively low growth temperature of the $Cd_{0.9}Zn_{0.1}O$ NPs compared to the growth and process temperatures found in GaAs-based technology ensures that the NPs can be integrated on QWIPs. Moreover, this concept can be extrapolated to other material platforms absorbing in the 3–6 μm range, like the case of PbSe, InSb, or HgCdTe photodetectors [8].

The MQW structure consists of 5× GaAs/$Al_xGa_{1-x}As$ QWs, where the QW width and barrier alloy composition have been varied to tune the intersubband transition frequency (ω_{12}) with that of the LE and HE plasmonic modes. Since the MQWs are designed to be part of a QWIP, the second level is placed close to the continuum in order to allow the extraction of the electrons from the QW [28]. The ω_{12} values were calculated numerically directly from self-consistent solution of the Schrodinger and Poisson equations, including depolarization effects [29, 30]. All material parameters for GaAs and $Al_xGa_{1-x}As$ are taken from the literature [31].

In the case of the MQWs tuned to match the HE mode, a 3.4 nm-thick GaAs QW doped to 1×10^{19} cm^{-3} and a 4 nm-thick AlAs barrier is used, yielding an intersubband absorption resonance at 3750 cm^{-1}. For the MQW structure tuned to match the LE mode, a 5 nm-thick GaAs QW doped to 4.2×10^{18} cm^{-3} is used with a 4 nm-thick $Al_{0.35}Ga_{0.65}As$, yielding an intersubband absorption resonance at 1774 cm^{-1}. The thickness of the barrier ensures that the QWs are electronically uncoupled.

In order to model the interaction of the LE/HE plasmonic modes with the MQWs, an anisotropic dielectric function is used for the QW. This function has a Drude term in the in-plane direction accounting for the plasma resonance, and a Lorentz oscillator in the out-of-plane direction accounting for the fact that the intersubband transition can only be excited by light polarized perpendicular to the in-plane direction [32], and is defined as follows:

$$\varepsilon^{\mathrm{GaAs}}_{\mathrm{in-plane}}(\omega)=\varepsilon^{\mathrm{GaAs}}_{\infty}\left(1-\frac{\omega_P^2}{\omega^2+i\omega\gamma^P_{\mathrm{in-plane}}}\right) \tag{2}$$

$$\varepsilon^{\mathrm{GaAs}}_{\mathrm{out-of-plane}}(\omega)=\varepsilon^{\mathrm{GaAs}}_{\infty}\left(1+\frac{f_{12}\omega_P^2}{\omega_{12}^2-\omega^2-i\omega\gamma^P_{12}}\right) \tag{3}$$

Here, ω_p is the in-plane plasma frequency and $\gamma^P_{\mathrm{in-plane}}$ its broadening, f_{12} is the intersubband oscillator strength, ω_{12} the intersubband frequency, and γ_{12} its broadening. For this simulation we have assumed a broadening of 10% the value of the plasma/intersubband frequencies, which are typically found in state of the art GaAs-based technology.

In contrast, the $Al_xGa_{1-x}As$ barrier is modeled as a dielectric material with an isotropic function:

$$\varepsilon^{\mathrm{AlGaAs}}_{\mathrm{in-plane}}(\omega)=\varepsilon^{\mathrm{AlGaAs}}_{\mathrm{out-of-plane}}(\omega)=\varepsilon^{\mathrm{AlGaAs}}_{\infty} \tag{4}$$

In all cases, the contribution of phonons to the dielectric function has been neglected, since the phonons are found at much lower frequencies than the LE and HE modes, and thus, do not have an effect on the coupling results.

As previously discussed, only the out-of-plane component of the electric field can be absorbed by QWs due to the selection rules. Figure 5 shows that for this component of the electric field a large amplification in the MQW absorption is provided both by the LE and HE modes. This is especially relevant in the case of the LE mode where an enhancement factor around 2 is still maintained well below 50 nm. In the HE mode, the plasma oscillations provide a smaller out-of-plane component, but it is still significant when compared to its negligible value without NPs. Figure 5 also shows that the gain provided by both modes extends down to 75–100 nm,

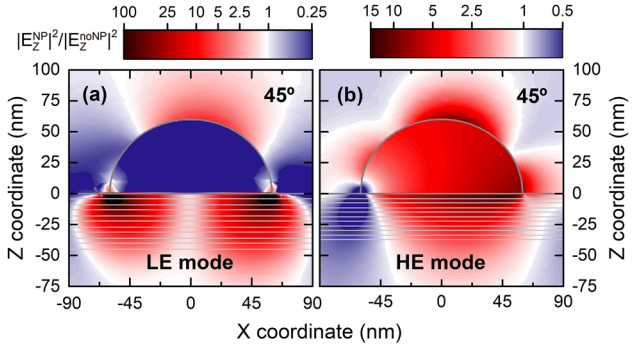

Figure 5: Enhancement of the squared *z*-component of the electric field in MQWs, defined as the ratio of $|E_z|^2$ with and without NPs, at 45°. (a) LE resonant MQWs. (b) HE resonant MQWs. The 5× alternating barrier-QW periods are represented below the NP base.

allowing to couple the plasmonic modes to thicker structures.

The large gains are easily explained considering the high refractive index of the materials that constitute the quantum wells and the barriers. Even for large angles of incidence, the strong light refraction prevents the out-of-plane electric field component to be significant within the GaAs MQWs. This is also true for the LE mode, where the z-amplification is even larger due to the strong field divergence around the NP edges.

In order to quantify the enhancement in the MQW power absorption that is provided by the NPs, the NP surface coverage has been changed depending on the mode. For the LE mode, we assume a NP surface coverage of 32%, the same value as one of our experimental samples. This amount of surface coverage takes full advantage of the LE mode, since this mode extends both vertically and laterally in the substrate, avoiding the loss of in-plane plasma confinement when the NPs coalesce. Since the modeled MQW structure is 45 nm-thick, it overlaps well with the region where there is amplification (Figure 5(a)), maximizing the improvement in power absorption.

Figure 6(a) compares the light absorption of the bare MQWs at normal incidence with the NP-enhanced case. Note that under this angle of incidence, the light is effectively *s*-polarized. As expected, no absorption occurs under normal incidence when there are no NPs. However, when covered with NP coatings, the MQWs show a large intersubband absorption at normal incidence when the intersubband frequency matches the LE mode, without the need for gratings and complex lithographic processes [8]. Indeed, the total absorbed power is comparable to that absorbed by the MQW at an angle of incidence of 45° (Figure 6(c)). At this angle, the NPs are responsible for an enhancement of the MQWs peak absorption by a factor as large as 5.5.

The LE mode covers well the 3–7 μm range, and provides a gain that compares quite well to that typically obtained by using diffraction gratings in QWIP focal plane arrays [33]. Indeed, gratings improve the normal incidence responsivity

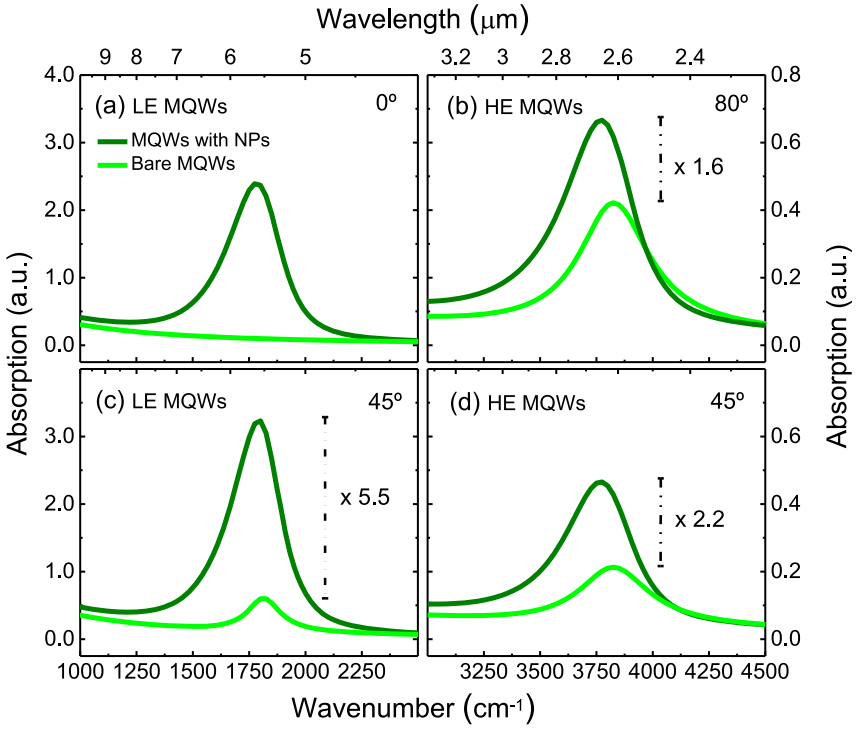

Figure 6: Light absorption enhancement in (a) MQWs coupled with the LE plasmonic mode at normal incidence; (b) MQWs coupled with the HE mode at 80°; (c) MQWs coupled with the LE mode at 45°; and (d) MQWs coupled with the HE mode at 45°. NP surface coverages of 32 and 75% are used when coupling the MQW structures to the LE and HE modes, respectively. The absorption units can be compared among panels.

of QWIPs by a factor of 2–3 with respect to the case of light propagating at 45°, lower than the 5.5-fold enhancement provided by the CdZnO NPs. Moreover, and as discussed in [9], infrared photodetectors can also benefit from their integration with plasmonic structures by decreasing their thermal noise while maintaining their responsivity, which can be realized decreasing the total active volume of the detector and preserving the total absorbed light power. In our case, the 45 nm-thick 5-well structure covered with NPs provides as much absorbed light power as an equivalent 225 nm-thick 25-well structure without NPs, but using an active region that is a factor of 5 thinner. Thus, the NP-enhanced photodetector with the thinner active region would present lower thermal noise and larger detectivity [8].

While the HE mode provides lower amplification than the LE one, it still shows potential for device applications in the 2–3 μm region. If we consider the large energy gap separating both modes, the range of tunability of the LE mode can hardly reach the energy of the HE mode. Thus, for lower wavelengths, the LE mode may not be an option. In order to analyze the HE mode, and since the electric field is only enhanced in the substrate below the NP and not around the edges (Figures 4(d) and 5(b)), the best-case scenario to take full benefit from it is to assume that the NPs are close to each other, with a high NP surface coverage. Figure 6(b) and (d) shows the enhancement in the light absorption of a MQW structure after covering 75% of the surface with $Cd_{0.9}Zn_{0.1}O$ NPs, close to the coalescence limit in a periodic square NP-lattice. The results of the enhancement of the MQWs absorption due to the LSPs from the NPs are still remarkable, yielding factors of 2.2 and 1.6 at 45° and 80°, respectively, at the resonant energy.

Our results are in line with those reported by various authors for different types of gold plasmonic-enhanced mid-IR photodetectors. In the work by Wu et al. [34], the use of periodically-microperforated gold layers on InGaAs QWIPs yielded an improvement in responsivity (which is proportional to absorption) of ×2.3. A similar gold-based microhole approach was carried out by Yakimov et al. on Ge/Si quantum dot infrared photodetectors (QDIPs) [35] resulting in ×4 gains in photocurrent. In addition to processed gratings, some discrete gold structures have also been shown to be successful as field enhancers in the visible and UV [13]. However, in such isolated metallic nanostructures, the LSPs are far from the IR due to the high electronic density in metals, and thus, the approach cannot be extended to the mid-IR.

Therefore, when compared to the metal-based approaches, the advantages of CdZnO are clear. Complex lithography processes to fabricate structured patterns are avoided due to the self-assembled nature of the NPs. In addition to this, and since most of the reported gold structures are gratings in the micrometric scale, much larger than the NP size, our approach has the potential to be compatible with them. Thus, the NPs could be deposited on top of a gold grating to further increase the absorption.

Next, we show experimentally the coupling of the NP LE plasmonic mode to the intersubband transitions, which results not only in enhanced absorption from the intersubband transitions under *p*-polarization, as mentioned above, but also intersubband absorption under *s*-polarization. We recall that intersubband transitions by themselves cannot absorb light under *s*-polarization. However, as discussed above, the hemispherical NPs allow to break this selection rule by providing light polarized in the *z*-direction (out-of-plane). Therefore, the observation of intersubband absorption under *s*-polarization serves to demonstrate the coupling.

For this experiment we have grown by Molecular Beam Epitaxy (MBE) a 15× GaAs/AlAs MQW structure on semi-insulating GaAs, which contains 5.5 nm-thick QWs doped 1×10^{18} cm^{-3}, and 3.6 nm-thick AlAs barriers. The calculated intersubband transition is centered at 2130 cm^{-1}, close to resonance with the LE plasmonic mode, which as discussed above, yields the largest amplification of the two plasmonic modes. Since the intersubband absorption in these systems is commonly too weak to be directly measured by transmittance experiments through the surface, a 45° waveguide configuration was used [28]. Under this configuration, light enters the waveguide at normal incidence and suffers multiple internal reflections at 45°, maximizing the absorption by the QWs (Figure 7(a)). Indeed, the MQW waveguide shows a sharp, well-defined minimum at 2170 cm^{-1} when illuminated with *p*-polarized light, corresponding to the intersubband transitions from the MQWs (Figure 7(b)). Under *s*-polarization, and as dictated by the absorption selection rules, no intersubband absorption is observed.

Subsequently, CdZnO NPs were deposited on top of the same waveguide containing MQWs, as well as on a second waveguide without MQWs, which serves as a reference. The waveguides showed a NP surface coverage around 29%, close to the 32% sample presented earlier. Figure 7(c) shows the transmittance spectra of the reference waveguide where the LE plasmonic mode is clearly observed for both *p*- and *s*-polarizations. As expected, for the LE mode, absorption by the NPs is present under *s*-polarization, where the electric field is polarized parallel to the substrate/NP interface, and is of the same magnitude as under *p*-polarization. This behavior is in stark contrast to that of intersubband transitions.

Figure 7(d) shows the waveguide transmittance spectrum of the MQWs after the growth of the NPs. A clear minimum is observed, matching the one found for the

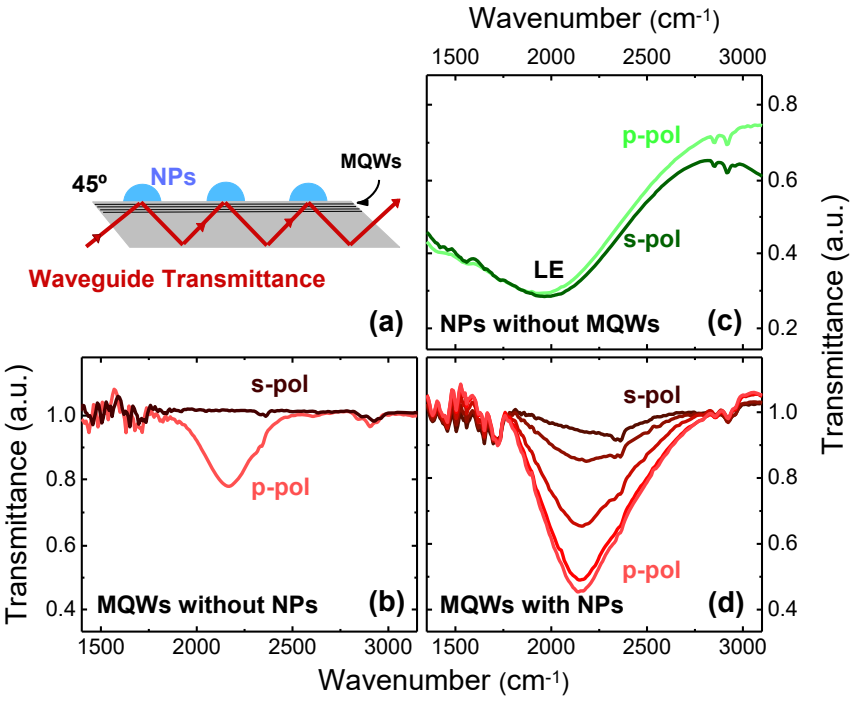

Figure 7: (a) Configuration for the waveguide transmittance measurements. (b) to (d): Waveguide transmittance of the MQW sample prior to growth of the NPs (b), the reference sample with NPs and without MQWs (c), and the same MQW sample from (b) after growth of the NPs (d). By rotating the external polarizer by 90° the polarization of the incident light respect to the MQWs is changed from purely *s*-polarized, to purely *p*-polarized. Each step in the color gradient in (d) corresponds to a 22.5° rotation of the polarizer. Units in (b) and (d) can be compared.

intersubband transition prior to the growth of the NPs (Figure 7(b)). In addition, the polarization-dependent behavior of the minimum clearly follows the pattern associated with the intersubband transition and, as previously discussed, is not compatible with the response of the LE mode (Figure 7(c)). Hence, this absorption minimum cannot be explained as an effect of the NPs alone, and its behavior is clearly in agreement with the intersubband transition. On the other hand, differences with the absorption from the bare MQWs presented in Figure 7(b) are also evident. Upon the growth of the NP on top of the MQWs, the intensity of the intersubband transition is multiplied by a factor close to 2.5, consistent with the amplification of the field by the NPs. In addition, its broadening is increased by a factor close to 80%, but it still much smaller than that from the LE mode alone (Figure 7(c)). This would be expected for a coupled system, where the intersubband transition is clearly affected by the larger broadening of the LE mode. Finally, absorption is observed even under *s*-polarization, as predicted by the model in Figure 6(a) and expected from the reorientation of the electric field around the edges of the NPs. Therefore, the experimental results show solid evidence of the coupling between the NP plasmonic resonance and the intersubband transition, whose response is increased in intensity and broadening, becoming allowed even for *s*-polarized light.

For future QWIP applications there are some technological challenges that would need to be considered. To help placing the active MQWs in the region where the field amplification takes places, the top n^+-contact layer needs to be reduced as much as possible, or even alternative geometrical configurations need to be used. Even though this may increase the series resistance of the QWIP, it should not be a limiting factor because the total current that flows in this type of devices is quite low [28]. Moreover, since the QWIP n^+-contact layer is typically doped to $1–3 \times 10^{18}$ cm^{-3}, its associated plasma reflectance will fall well below the spectral region where the LE and HE plasmonic modes are found, and the contact layer will thus behave as a dielectric having no effect on the propagation of light.

Finally, maximum benefit from the results here presented can be obtained under two configurations. One option is to increase the responsivity of QWIPs with a small number of QWs, or even to use a single QW [28]. Indeed, single quantum well QWIPs are especially interesting for high speed detection, where the electrons are injected in the QW through tunneling, but due to the low number of QWs they suffer from low responsivity. Placing the single QW in the region where the plasmonic amplification takes place could allow to increase it by a factor of 5. Alternatively, CdZnO NPs can be used in QWIPs with thicker active regions. Some of the topmost QWs would experience increased absorption, which can allow for smaller number

of QWs, and therefore reduced thickness while maintaining the responsivity and yielding an increased detectivity.

5 Conclusion

In summary, we have experimentally demonstrated that LSP modes arise in $Cd_{0.9}Zn_{0.1}O$-based hemispherical NPs, which are governed by the geometry of the NPs, and allowed by their high plasma frequency and low optical losses. Two sharp LSP modes appear in the mid-IR, located at 5.3 and 2.7 μm, which strongly enhance the electric field in the underlying GaAs. The LE mode (at 5.3 μm) shows very strong light amplification, with intensity gain above 100 just below the NPs and sustained amplification down to 50 nm. Although the plasma oscillations in the NP occur parallel to the NP-substrate interface, the strong divergence of the electric field around the edges of the hemispherical NP also gives rise to a strong out-of-plane component in the underlying GaAs. The presence of both in-plane and out-of-plane electric field components opens the door to its coupling to a wide variety of IR absorbing systems, including isotropic absorbers (like small bandgap materials) and polarization-selective ones (like QWs).

In the case of the HE mode (at 2.7 μm), within the NP the plasma oscillations are highly polarized in the out-of-plane direction and most of the amplification appears at the apex of the NP. Nevertheless, there is some amplification of the light intensity in the GaAs substrate, which is as large as a factor of 2 down to 50 nm at 45° incidence if only the out-of-plane component of the field is considered.

The coupling of these modes to intersubband transitions in GaAs-based MQWs and the improvement in the total absorbed light power by the MQWs was also considered. In a 5-QW system, coupling to the LE mode enhanced the absorbed light power by a factor of 5.5 (when compared to bare MQWs at 45°), allowing also normal incidence absorption thanks to the strong field divergence at the NP edges. Under similar conditions, the HE mode provides a power absorption gain in the MQWs of 2.2.

Beyond the numerical analysis, the coupling between intersubband transitions and the LE plasmonic mode was also demonstrated. CdZnO NPs were grown on a sample containing a 15× GaAs/AlAs MQW structure. The optical analysis showed a clear enhancement in the absorption of the coupled system with MQWs and NPs grown on top, with a gain around a factor of 2.5 and increased broadening when compared to the bare MQWs. In addition, and as predicted by the model, plasmon-coupled intersubband absorption is also observed for illumination with *s*-polarized light. This situation is analogous to absorption at normal incidence, and together with the enhanced absorption under *p*-polarization, provides proof of the coupling between the LSP mode and the intersubband transition.

In addition to the large enhancement in the absorption of mid-IR light, the fact that the CdZnO-based NPs can be grown through a self-assembled process and at relatively low temperatures provides a solid ground for their integration on different infrared photodetector platforms, and particularly on GaAs-based QWIP focal plane arrays. Additionally, and contrary to the case of noble metals, the energy of the plasmonic resonances can be further tuned by doping or alloying the metal-oxide NPs, increasing the spectral range where this approach can be used.

6 Supplementary Material

Section 1. Discusses the validity of Drude's model in the description of CdZnO. Experimental evidence is included showing that this model accurately describes the optical behavior of CdO.

Section 2. Discusses the geometrical details considered for the FDTD model, including spectrum variability derived from the inclusion of different NP shapes and sizes.

Section 3. Adds a study of a new series of NPs to verify the reproducibility of the NP growth.

Section 4. Includes the band structures of all the MQW systems used in this paper.

Acknowledgements: E. Martínez Castellano and J. Yeste hold an FPU (Formacion de Profesorado Universitario) predoctoral contract from the Spanish Ministry of Science, Innovation and Universities (MICIU). L. Stanojević holds a predoctoral contract from Universidad Politécnica de Madrid.

Author contributions: All the authors have accepted responsibility for the entire content of this submitted manuscript and approved submission.

Research funding: This work was funded by the Spanish Ministry of Economy, Industry and Competitiveness (MINECO) under Project TEC2017-85912-C2, and the Generalitat Valenciana under project Prometeo II 2015/004.

Conflict of interest statement: The authors declare no conflicts of interest regarding this article.

References

[1] M. I. Stockman, K. Kneipp, S. Bozhevolnyi, et al., "Roadmap on plasmonics," *J. Opt.*, vol. 20, no. 4, p. 043001, 2018.

[2] H. T. Chen, A. J. Taylor, and N. Yu, "A review of metasurfaces: physics and applications," *Rep. Prog. Phys.*, vol. 79, no. 7, 2016, https://doi.org/10.1088/0034-4885/79/7/076401.
[3] A. Li, S. Singh, and D. Sievenpiper, "Metasurfaces and their applications," *Nanophotonics*, vol. 7, no. 6, pp. 989–1011, 2018.
[4] A. Dorodnyy, Y. Salamin, P. Ma, et al., "Plasmonic photodetectors," *IEEE J. Sel. Top. Quant. Electron.*, vol. 24, no. 6, pp. 1–13, 2018.
[5] T. Taliercio and P. Biagioni, "Semiconductor infrared plasmonics," *Nanophotonics*, vol. 8, no. 6, pp. 949–990, 2019.
[6] A. Boltasseva and H. A. Atwater, "Low-loss plasmonic metamaterials," *Science*, vol. 331, no. 6015, pp. 290–291, 2011.
[7] H. Khamh, E. Sachet, K. Kelly, J.-P. Maria, and S. Franzen, "As good as gold and better: conducting metal oxide materials for mid-infrared plasmonic applications," *J. Mater. Chem. C*, vol. 6, no. 31, pp. 8326–8342, 2018.
[8] A. Rogalski, *Infrared Detectors*, 2nd ed. Boca Raton, FL, CRC Press, 2010.
[9] R. Stanley, "Plasmonics in the mid-infrared," *Nat. Photonics*, vol. 6, no. 7, pp. 409–411, 2012.
[10] W. L. Barnes, A. Dereux, and T. W. Ebbesen, "Surface plasmon subwavelength optics," *Nature*, vol. 424, no. 6950, pp. 824–830, 2003.
[11] A. Sobhani, M. W. Knight, Y. Wang, et al., "Narrowband photodetection in the near-infrared with a plasmon-induced hot electron device," *Nat. Commun.*, vol. 4, pp. 1643–1646, 2013.
[12] S. C. Lee, S. Krishna, and S. R. J. Brueck, "Quantum dot infrared photodetector enhanced by surface plasma wave excitation," *Opt. Express*, vol. 17, no. 25, p. 23160, 2009.
[13] M. Chen, L. Shao, S. V. Kershaw, et al., "Photocurrent enhancement of HgTe quantum dot photodiodes by plasmonic gold nanorod structures," *ACS Nano*, vol. 8, no. 8, pp. 8208–8216, 2014.
[14] V. Amendola, R. Pilot, M. Frasconi, O. M. Maragò, and M. A. Iatì, "Surface plasmon resonance in gold nanoparticles: A review," *J. Phys. Condens. Matter*, vol. 29, no. 20, p. 203002, 2017.
[15] B. Doiron, M. Mota, M. P. Wells, et al., "Quantifying figures of merit for localized surface plasmon resonance applications: A materials survey," *ACS Photonics*, vol. 6, no. 2, pp. 240–259, 2019.
[16] P. R. West, S. Ishii, G. V. Naik, N. K. Emani, V. M. Shalaev, and A. Boltasseva, "Searching for better plasmonic materials," *Laser Photon. Rev.*, vol. 4, no. 6, pp. 795–808, 2010.
[17] J. D. Caldwell, L. Lindsay, V. Giannini, et al., "Low-loss, infrared and terahertz nanophotonics using surface phonon polaritons," *Nanophotonics*, vol. 4, no. 1, pp. 44–68, 2015.
[18] E. Sachet, C. T. Shelton, J. S. Harris, et al., "Dysprosium-doped cadmium oxide as a gateway material for mid-infrared plasmonics," *Nat. Mater.*, vol. 14, no. 4, pp. 414–420, 2015.
[19] E. L. Runnerstrom, K. P. Kelley, T. G. Folland, et al., "Polaritonic hybrid-epsilon-near-zero modes: beating the plasmonic confinement vs propagation-length trade-off with doped cadmium oxide bilayers," *Nano Lett.*, vol. 19, no. 2, pp. 948–957, 2019.
[20] J. Tamayo-Arriola, E. Martínez Castellano, M. Montes Bajo, et al., "Controllable and highly propagative hybrid surface plasmon–phonon polariton in a CdZnO-based two-interface system," *ACS Photonics*, vol. 6, no. 11, pp. 2816–2822, 2019.
[21] J. Tamayo-Arriola, A. Huerta-Barberà, M. Montes Bajo, et al., "Rock-salt CdZnO as a transparent conductive oxide," *Appl. Phys. Lett.*, vol. 113, no. 22, p. 222101, 2018.
[22] V. M. Ustinov and A. E. Zhukov, "GaAs-based long-wavelength lasers," *Semicond. Sci. Technol.*, vol. 15, no. 8, pp. R41–R54, 2000.
[23] Z. Li, H. H. Tan, C. Jagadish, and L. Fu, "III-V semiconductor single nanowire solar cells: A review," *Adv. Mater. Technol.*, vol. 3, no. 9, p. 1800005, 2018.
[24] D. Strauch and B. Dorner, "Phonon dispersion in GaAs," *J. Phys. Condens. Matter*, vol. 2, no. 6, pp. 1457–1474, 1990.
[25] S. A. Maier, "Localized surface plasmons," in *Plasmonics: Fundamentals and Applications*, New York, NY, Springer US, 2007.
[26] T. Skauli, P. S. Kuo, K. L. Vodopyanov, et al., "Improved dispersion relations for GaAs and applications to nonlinear optics," *J. Appl. Phys.*, vol. 94, no. 10, pp. 6447–6455, 2003.
[27] D. Palaferri, Y. Todorov, A. Bigioli, et al., "Room-temperature nine-μm-wavelength photodetectors and GHz-frequency heterodyne receivers," *Nature*, vol. 556, no. 7699, pp. 85–88, 2018.
[28] H. Schneider and H. C. Liu, *Quantum Well Infrared Photodetectors: Physics and Applications*, Berlin, Heidelberg, Springer-Verlag, 2007.
[29] M. Montes Bajo, J. Tamayo-Arriola, M. Hugues, et al., "Multisubband plasmons in doped ZnO quantum wells," *Phys. Rev. Appl.*, vol. 10, no. 2, p. 1, 2018.
[30] Aestimo self-consistent Schrödinger-Poisson solver for semiconductor heterostructures (ver. 1.2). Available at: http://www.aestimosolver.org/ [Downloaded: Dec. 1, 2017].
[31] S. Adachi, *Properties of Semiconductor Alloys*, Chichester, UK, John Wiley & Sons, Ltd, 2009.
[32] W. P. Chen, Y. J. Chen, and E. Burstein, "The interface EM modes of a 'surface quantized' plasma layer on a semiconductor surface," *Surf. Sci.*, vol. 58, no. 1, pp. 263–265, 1976.
[33] S. D. Gunapala and S. V. Bandara, "Chapter 4 quantum well infrared photodetector (QWIP) focal plane arrays," *Semiconduct. Semimet.*, vol. 62, no. C, pp. 197–282, 1999.
[34] W. Wu, A. Bonakdar, and H. Mohseni, "Plasmonic enhanced quantum well infrared photodetector with high detectivity," *Appl. Phys. Lett.*, vol. 96, no. 16, pp. 1–4, 2010.
[35] A. I. Yakimov, V. V. Kirienko, V. A. Armbrister, et al., "Surface plasmon dispersion in a mid-infrared Ge/Si quantum dot photodetector coupled with a perforated gold metasurface," *Appl. Phys. Lett.*, vol. 112, no. 17, 2018, https://doi.org/10.1063/1.5029289.

Supplementary Material: The online version of this article offers supplementary material (https://doi.org/10.1515/nanoph-2021-0167).